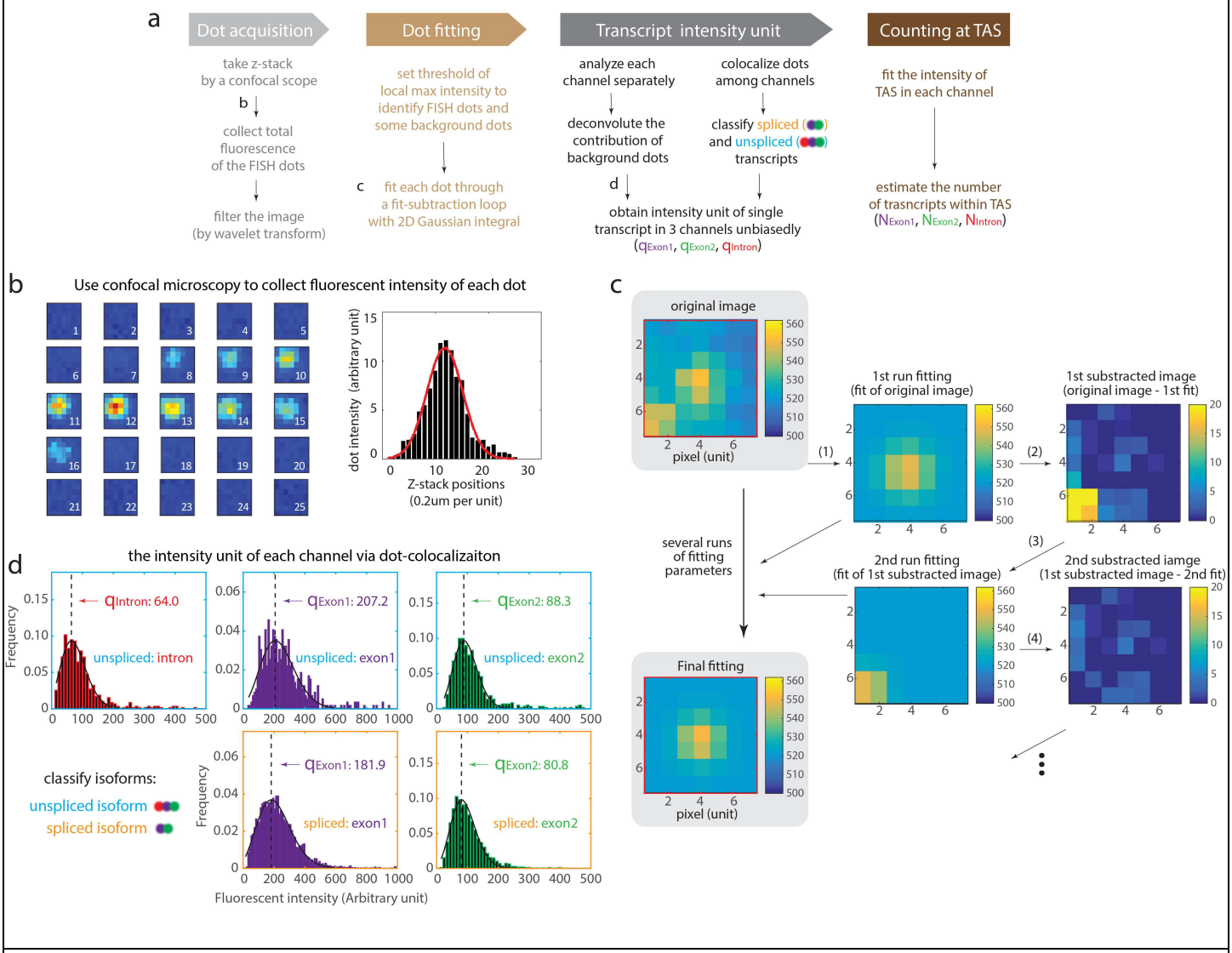

Supplementary Figure 1

Detailed workflow for quantifying the number of transcripts at the TAS. (a) The expanded version of Figure 2b. (b) The z-axis max projection of confocal images represents the intensity of the fluorescent FISH dots. (c) We fit the dot-intensity by a fit-subtraction loop. (1) Fit the dot with a 2D Gaussian intensity distribution; (2) Subtract the fitting from the original image and obtain a new image; (3) Fit the new image with another 2D Gaussian; (4) Subtract this new fitting from the new images. This fit-subtraction loop continues until the intensity of the new 2D Gaussian fitting falls below 10% of the first integrated dot intensity. Finally, the original image is fit by the sequential 2D Gaussian fit together, whose positions are constrained. (d) Analysis of dots co-occurring in multiple channels provides an alternative estimate of the single-molecule fluorescence unit. Here, each histogram includes only dots that appear in two or more channels. Poisson fitting of these intensity distributions generates similar single-molecule fluorescence units as in Figure 3b. Color is labeled as in Figure 2a.

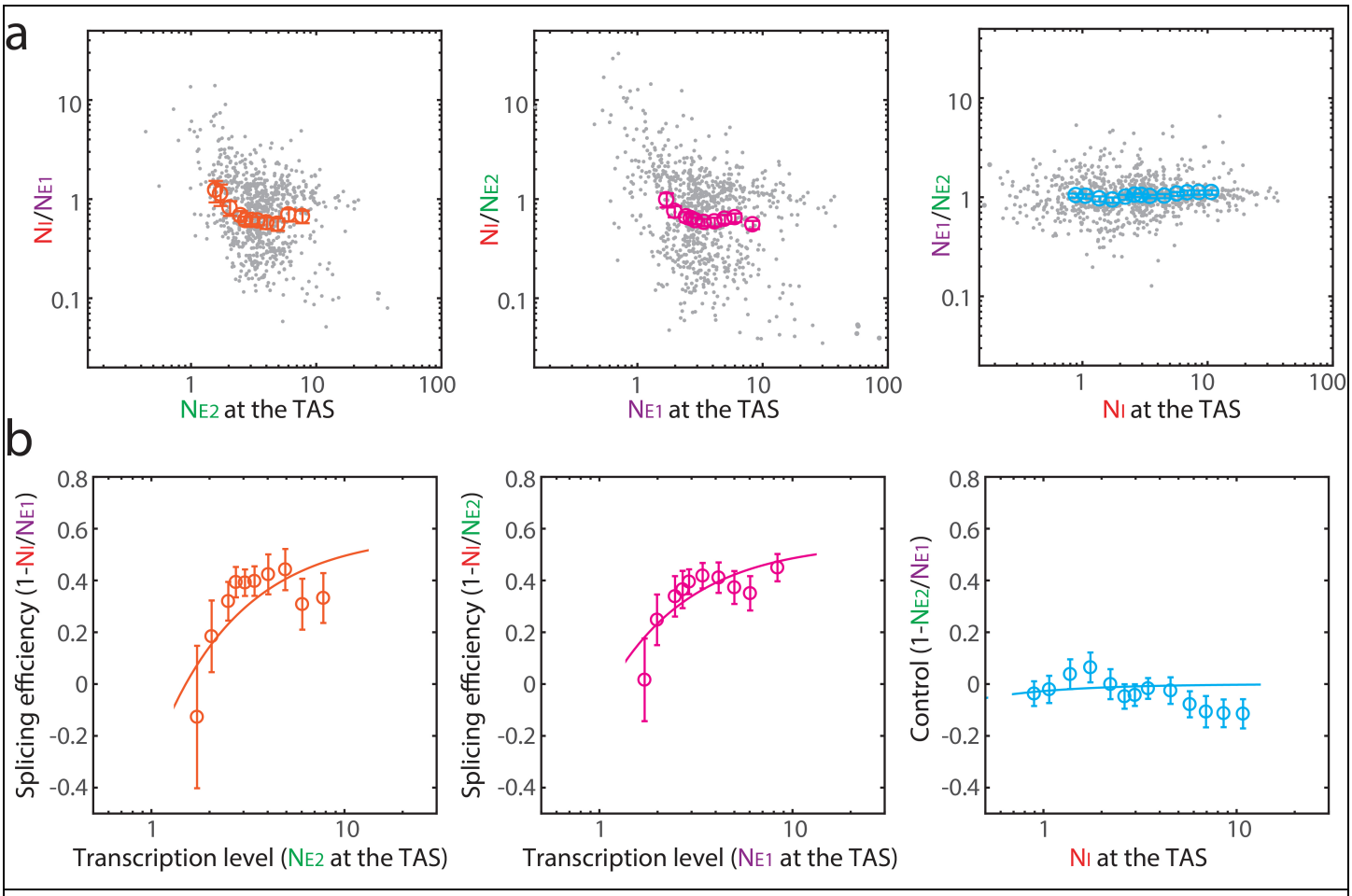

Supplementary Figure 2

Splicing efficiency increases with transcription level for RG6 genes induced by dox in HEK293 cells. Each dot is the measurement of a single TAS. Colors and labels are as in Figure 4.

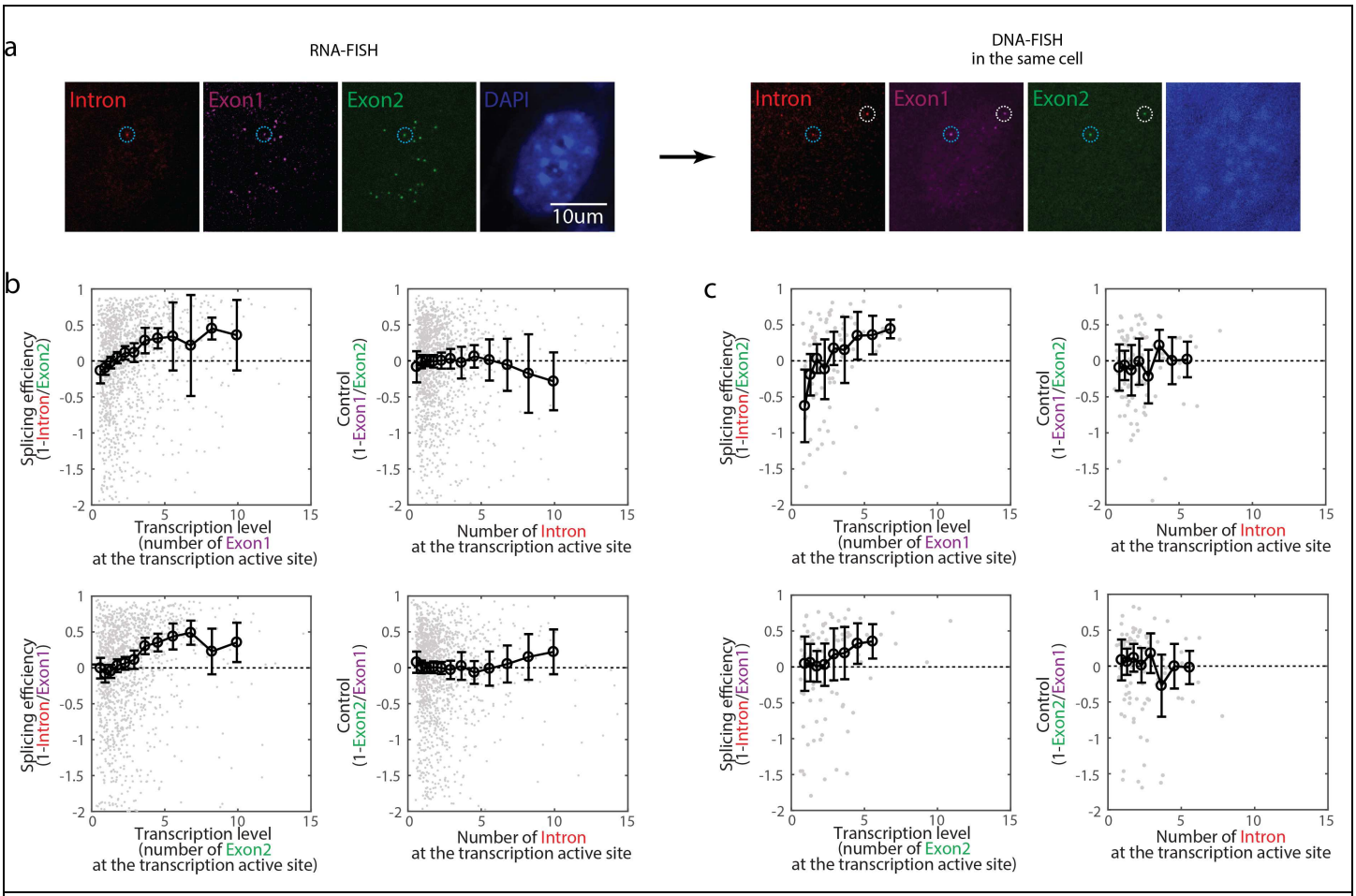

Supplementary Figure 3

DNA-FISH verifies the 'economy of scale' observation for Gli1. (a) We first performed RNA-FISH, labeling intron, Exon1, and Exon2, and then ran DNA-FISH in the same cells (see SI Materials and Methods for details). In the example image, DNA-FISH identified two genomic loci, while only one has co-localized dots in the RNA-FISH images. These results indicate that one locus (circled in white) is not active, while the other one (circled in blue) is active. (b) 'Economy of scale' observation based only on RNA-FISH images (n=1430). (c) The 'economy of scale' effect remains when considering only the TASs overlapping with DNA-FISH dots across three fluorescent channels (n=92). Note that we have significantly fewer measurements in this plot, due to the technical difficulty of combining DNA-FISH with RNA-FISH. Data are representative of two independent experiments.

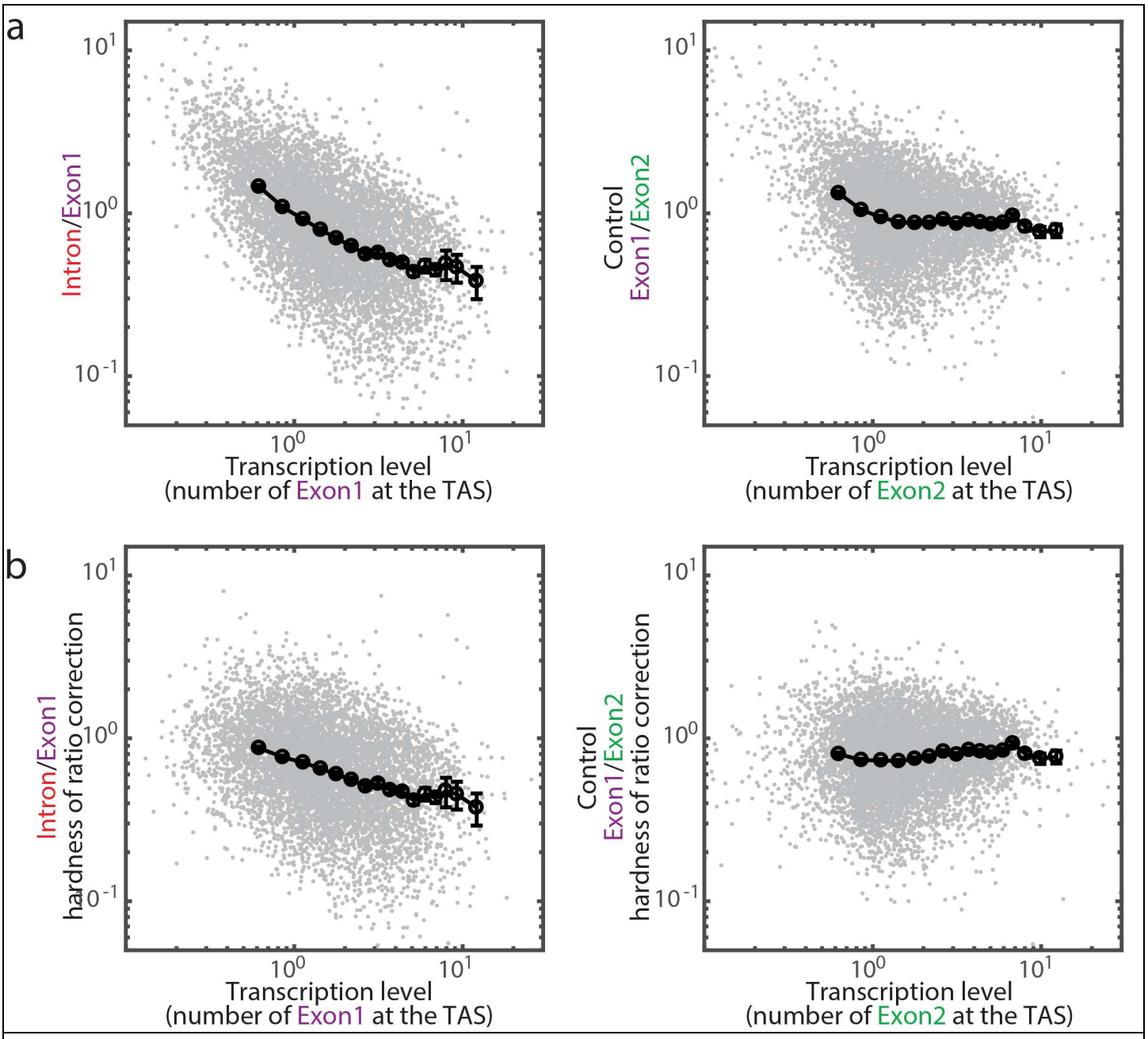

Supplementary Figure 4

Hardness of ratio correction. (a) False-positive 'economy of scale' for both splicing efficiency and control measurements, due to the putative correlation between denominator and numerator, i.e. $1 - N_I/N_{E1}$ versus N_{E1}. (b) Mathematical methods can correct this hardness of ratio with a = 4.3. The control measurements are, as expected, constant, while splicing efficiency still maintains the 'economy of scale' trend. See SI text for more details.

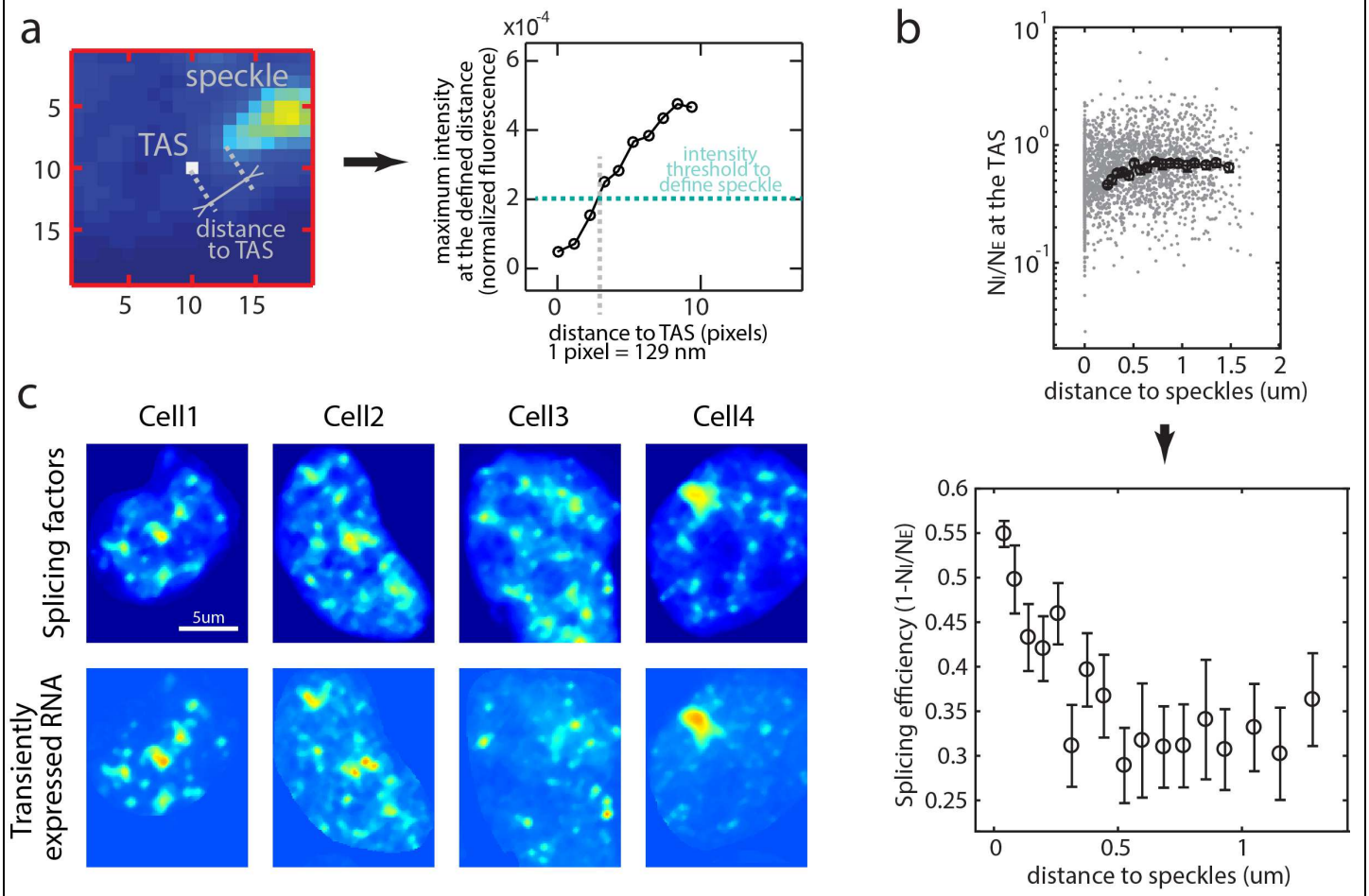

Supplementary Figure 5

(a) Measurement of the distance between a TAS and the nearest speckle. We first defined a set of fixed distances from the TAS. Specifically, we defined distance in units of pixels. Each circle (center panel) represents a defined distance from the TAS. Then, we measured the maximum fluorescent intensity at fixed distances. Finally, we plotted the maximum intensity versus the distance and found the minimum distance where the intensity reaches a pre-set threshold (right panel). (b) Raw data (n=2421) for Figure 5d. Error bars represent standard error of the mean. (c) The spatial distribution of splicing factors positively correlates with nascent splicing targets in HEK293 cells. Top: Splicing factors in the nucleus by citrine labeling Serine/arginine-rich splicing factor 1 (SRSF1); Bottom: RNA from transient transfection in the nucleus by FISHing intron. The cells have stably integrated citrine labelled SRSF1 gene and transiently transfected RNA (a synthetic SRSF1 targeted transcript, see Materials and Methods). The transient transfection generates multiple transcription active sites in the nucleus. As shown in the figure, the activities of these TASs are positively correlated with the proximity to speckles: every TAS is colocalized with a speckle and higher expressed TASs are with higher amount of splicing factors. Notice that some speckles do not have correlated TAS. This is because there are other TASs in the cell apart from the transiently transfected RNAs.

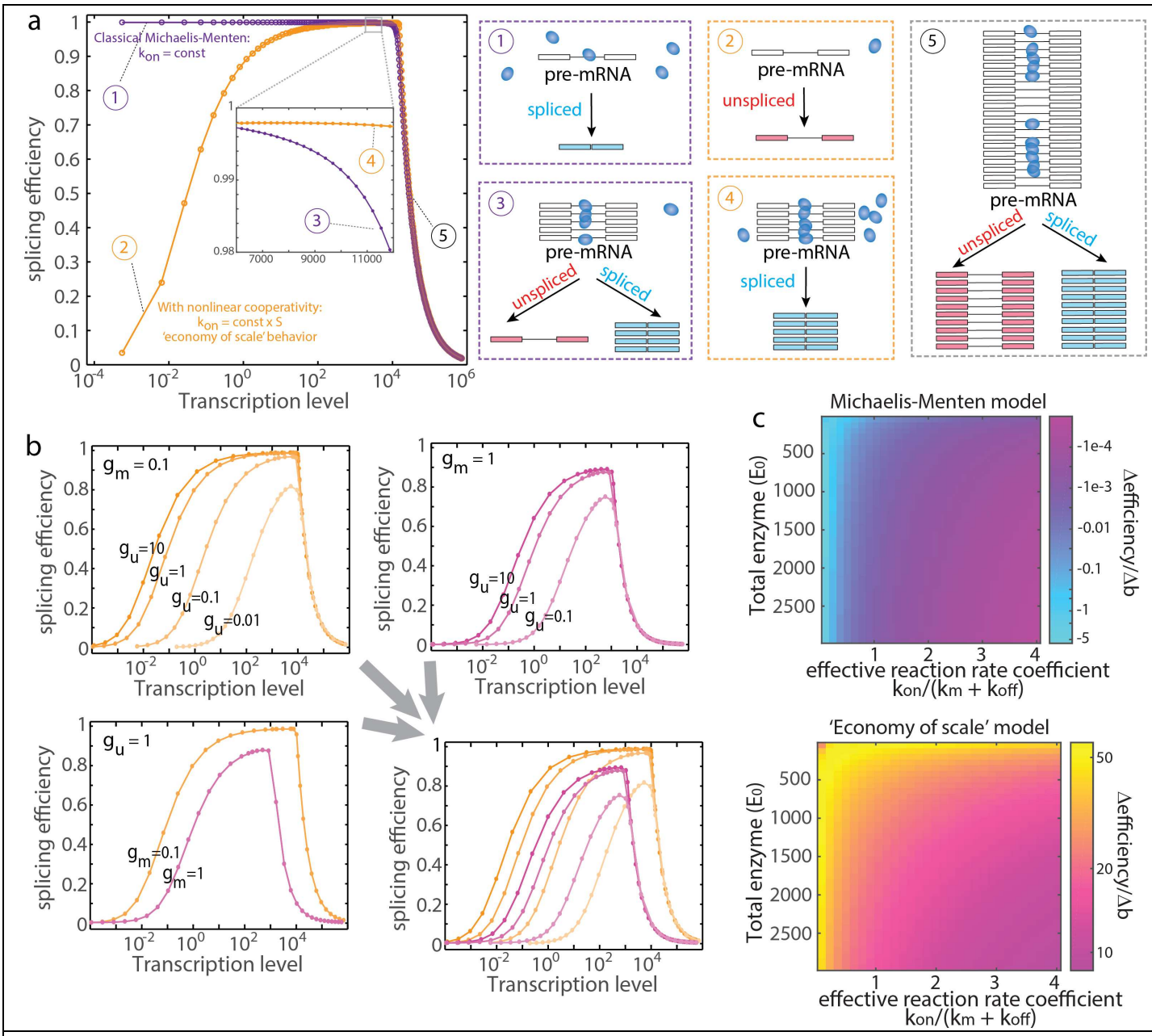

Supplementary Figure 6

A phenomenological mathematical model of the 'economy of scale' behavior. (a) Purple curve represents classical Michaelis-Menten model with uniform enzyme accessibility (i.e. constant k_{on}). Orange curve represents the modified model in which k_{on} is proportional to the available pre-mRNA concentration. For the classical model (purple curve), the splicing efficiency is close to 1 at low transcription levels (box 1), where enzyme levels are not limiting, and then decline at higher transcription levels (box 3) due to saturation. By comparison, for the modified model (orange curve), the splicing efficiency is close to 0 at low expression levels (box 2), where pre-mRNA concentrations are too low to recruit splicing machinery. As the transcription level increases (box 4), enzyme accessibility increases, and splicing efficiency increases to 1. This represents the observed 'economy of scale' effect. Further increases of transcription level eventually saturate the splicing machinery, reducing splicing efficiency (box 5). (b) 'Economy of scale' behavior is robust across different residence time (i.e. different degradation rate of unspliced and spliced isoforms, g_u and g_m respectively). Parameter values used here: $k_u = 0.1$, $k_m = 0.12$, rD = 100, $E_0 = 1000$ and $K = 0.5$. (c) 'Economy of scale' occurs across a wide range of parameters. The color scale, Δefficiency/Δb, represents the slope of splicing efficiency versus transcription level evaluated between b=1 and b=10. Pink to yellow (right) shows positive slope, i.e. 'economy of scale'; purple to blue (left) shows negative slope, i.e. 'diminishing returns.'

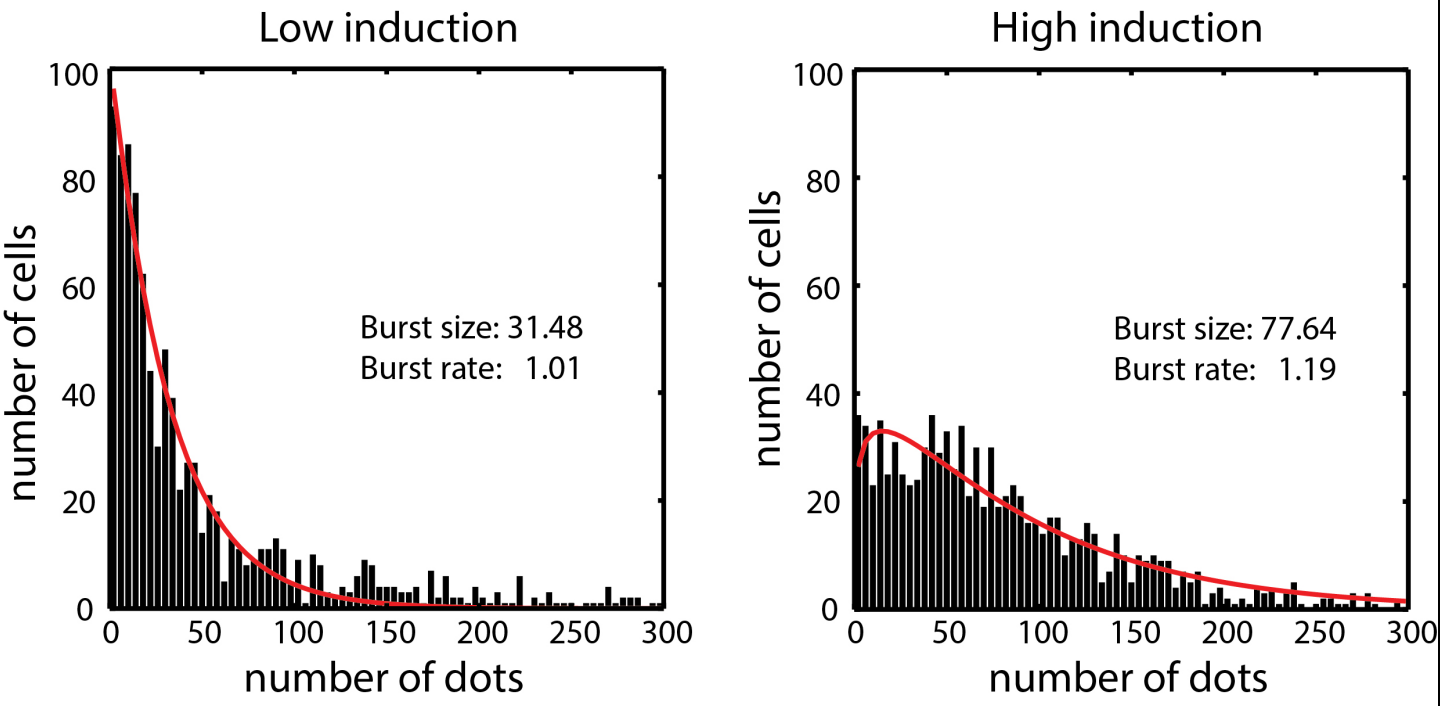

Supplementary Figure 7

The induction of promoter primarily affects transcriptional burst size. The synthetic mini-gene RG6 under Tet-on CMV was induced by 32 ng/ml (left panel) and 100 ng/ml (right panel) 4-Epidoxycycline (an analogue of Doxycycline). The distribution of mRNA expression (i.e. the number of smFISH dots) was fit by a previous published stochastic model (Raj, A., *et al*., *Nat. Methods* **5**, 877–879 2008).

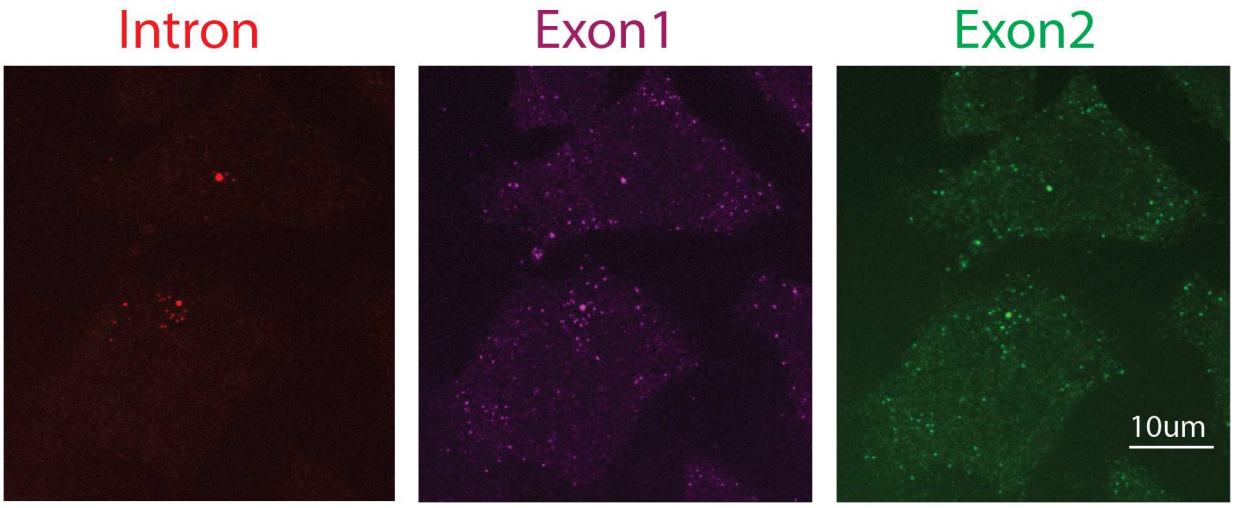

Supplementary Figure 8

Examples of different TASs. For the TAS in the bottom cell, transcripts are spreading out from the TAS, while for the TAS in the top cell, no obvious transcripts are seen in the neighborhood. Note that the two TASs have similar intensity (i.e. similar transcription level).

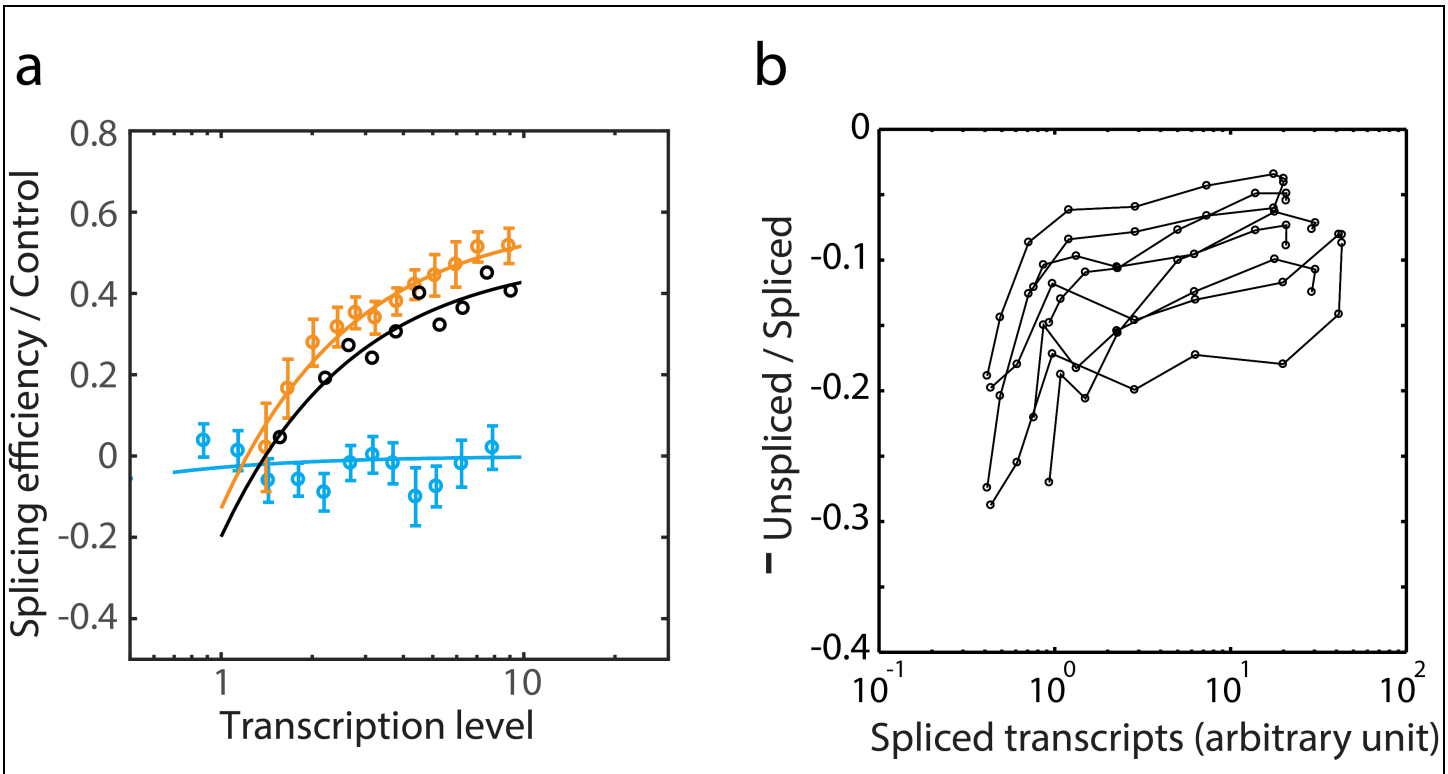

Supplementary Figure 9

(a) Ratio of the mean underestimates splicing efficiency. We calculated 1 - <Intron>/<Exon> (i.e. ratio of the mean) in black, as a comparison to the original 1 - <Intron/Exon> (i.e. mean of the ratio), same color as in Figure 4. Averaging over heterogeneous cells mildly distorts splicing efficiency (as illustrated in Figure 1), reducing the apparent magnitude of the 'economy of scale' effect. (b) Population-based measurements show the 'economy of scale' trend. We used qPCR to quantify the amounts of unspliced and spliced transcripts for RG6 (see Materials and Methods). Because qPCR does not provide absolute transcript abundances, we analyzed the ratio of unspliced to spliced abundances (each relative to a control gene) as a function of the relative abundance of spliced transcripts. Multiple curves represent repeats using different two different cell clones and multiple primer sets.

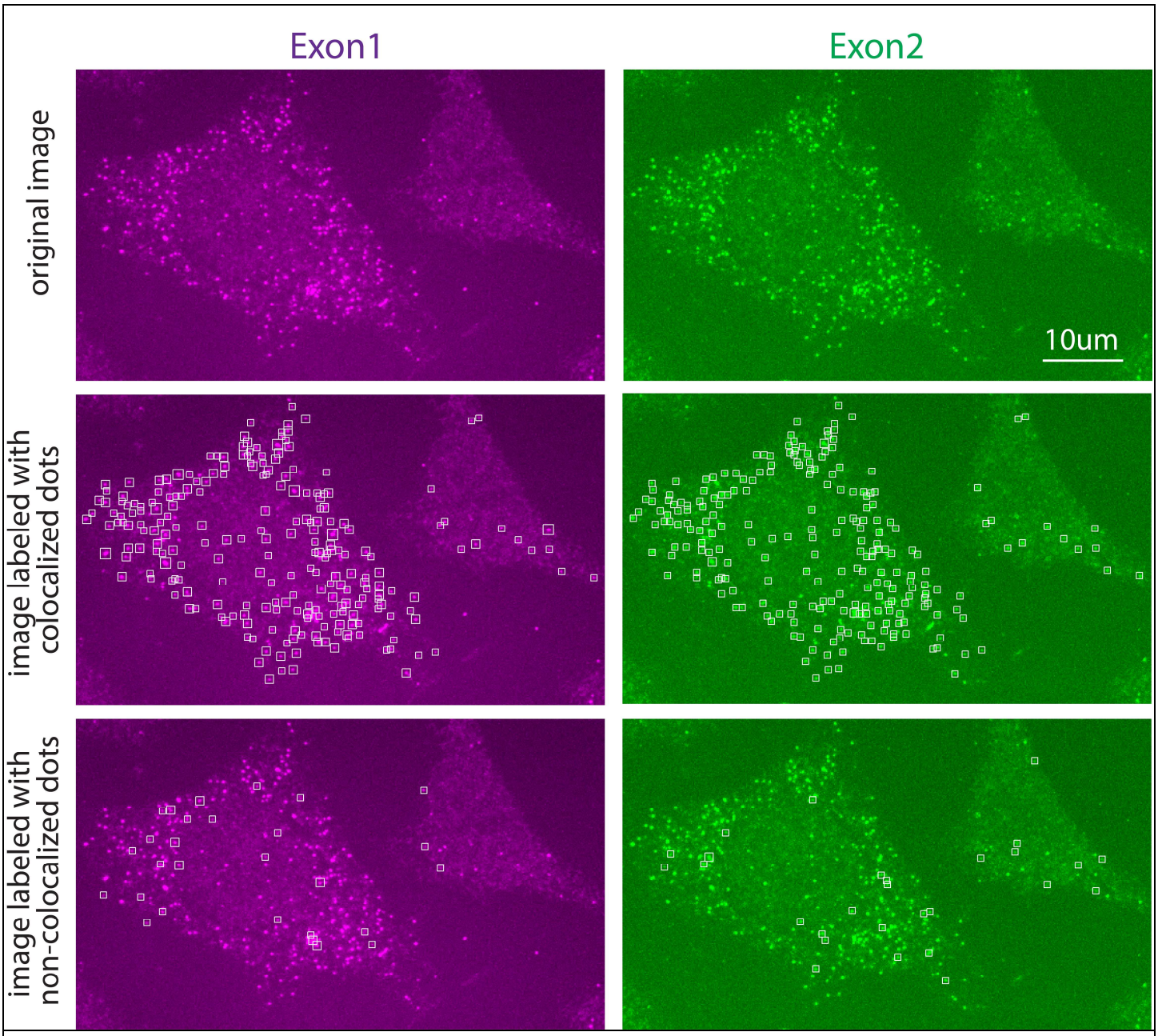

Supplementary Figure 10

Examples of co-localization of Exon1 and Exon2 probes. Top: Unprocessed images of both channels. Middle: all classified dots that co-localize in both channels are marked with white boxes. Bottom: Dots that were detected in only a single channel. Overall, the fraction of all dots that were co-localized between channels is ~90%.